Computer simulation of the energy dynamics of a sinusoidally perturbed double sine-Gordon equation: an application to the transmission of wave signals

J.E. Macías-Díaz
Departamento de Matemáticas y Física, Universidad Autónoma de Aguascalientes, Avenida Universidad 940, Ciudad Universitaria, Aguascalientes, Ags. 20131, Mexico, e-mail: jemacias@correo.uaa.mx

Recibido el 24 de septiembre de 2011; aceptado el 25 de noviembre de 2011

In this work, we employ a numerical method to approximate the solutions of a damped, double sine-Gordon equation spatially defined over a closed and bounded interval of the real line, subject to a harmonic perturbation of the Dirichlet type on one end, and a homogeneous Neumann condition on the other. The method has schemes to approximate consistently the temporal dynamics of the local energy density and the total energy of the medium, and the total energy over any finite interval of time and, additionally, it preserves the positivity of the corresponding energy operators. As an application of this method, we establish numerically that the phenomenon of nonlinear bistability (which is physically characterized by the coexistence of conducting and insulating regimes) is present in media governed by damped, double sine-Gordon equations when the systems are driven harmonically at a frequency in the forbidden band-gap. We employ this nonlinear process in order to accurately propagate localized pulses from the perturbed end to the free boundary. Two different methods for the transmission of monochromatic waves are employed in this study, and our results demonstrate that an efficient propagation of information is feasible, indeed.

Keywords: Double sine-Gordon equation; computer simulation; nonlinear bistability; wave propagation; signal transmission.

Este trabajo hace uso de una técnica numérica para aproximar las soluciones de un modelo amortiguado de doble seno-Gordon definido en un intervalo cerrado y acotado de números reales, sujeto a perturbaciones armónicas de Dirichlet en el extremo izquierdo, y condiciones homogéneas de Neumann en el derecho. El método incluye integradores para estimar consistentemente la dinámica temporal de la densidad local de energía, la energía total del modelo, así como la energía acumulada en intervalos finitos de tiempo; además, el método respeta la positividad de los correspondientes operadores de energía. Dicha técnica se aplica en la demostración computacional de la presencia del fenómeno de biestabilidad alineal (el cual se caracteriza físicamente por la coalescencia de regímenes conductores y aislantes) en medios descritos por ecuaciones amortiguadas de doble seno-Gordon y perturbados armónicamente por una frecuencia en el ancho de banda prohibido. Este proceso alineal es usado para propagar pulsos localizados del extremo perturbado a la frontera libre. Se proponen dos técnicas para la propagación confiable de ondas monocromáticas; los resultados de este trabajo indican que es posible transmitir la información de manera eficiente.

Descriptores: Ecuación de doble seno-Gordon; simulación computacional; biestabilidad alineal; propagación de ondas; transmisión de señales.

PACS: 46.15.-x; 02.60.Lj; 46.40.Cd; 05.45.Yv

1. Introduction

The class of nonlinear, hyperbolic partial differential equations identified as the *Klein-Gordon models*, is a well-known family of equations which finds applications in many physical problems. For example, a damped sine-Gordon equation appears in the study of long Josephson junctions between superconductors when dissipative effects are taken into account [1]. A similar partial differential equation with different nonlinear term appears in the study of fluxons in Josephson transmission lines [2]. Meanwhile, a modified Klein-Gordon equation appears in the statistical mechanics of nonlinear coherent structures such as solitary waves [3,4], assuming the form of a Langevin equation (see [5], pp. 298–309).

Klein-Gordon models have been studied extensively in the literature [6,7]. Moreover, the Klein-Gordon family has been a source of many interesting physical applications. For example, spatially discrete and continuous versions of this equations have been employed in the modeling of harmonic oscillators coupled through strings [8-10], in the design of digital amplifiers and sensors of ultra weak signals [11,12], in the investigation of Josephson transmission lines [2,13-15], and in the study of the dynamics of discrete Josehpson junctions coupled via superconducting wires [12]. Moreover, the spatially discrete version of the Klein-Gordon family in the form of a double sine-Gordon chain is also a topic of interest in view of the fact that this model exhibits the presence of the phenomenon of nonlinear bistability [16], a phenomenon which is also present in other nonlinear media [10-12].

In the context of electromagnetic theory, the process of *nonlinear bistability* is characterized by the coalescence of a conducting and an insulating regimes, particularly in media which are perturbed sinusoidally at one end at a frequency in the forbidden band-gap. Several physical models are known to exhibit the presence of the phenomenon of bistability, some of them being discrete Klein-Gordon and sine-Gordon systems [8,9], discrete β-Fermi-Pasta-Ulam chains [10], Bragg media in the nonlinear Kerr regime [17], and even spatially continuous, bounded media described by

undamped sine-Gordon equations [11]. Meanwhile, in the contexts of nonlinear optics and soliton physics, bistability refers to the existence of pairs of different soliton solutions for a common mathematical model under similar parametric circumstances [18-20].

It is important to mention that the models mentioned explicitly in the previous paragraph (Klein-Gordon, sine-Gordon and β-Fermi-Pasta-Ulam equations) exhibit the presence of two nonlinear phenomena: Supratransmission and infratransmission. *Nonlinear supratransmission* is a process characterized by a sudden increase in the amplitude of wave signals generated by the perturbed boundary, for driving amplitudes above a critical value called the *supratransmission threshold*. In fact, it has been established that spatially discrete double sine-Gordon chains do exhibit the presence of nonlinear supratransmission [9]; moreover, its occurrence has been predicted numerically in Ref. 16 via an energy-based computational method with multiple properties of consistency. *Nonlinear infratransmission*, as opposed to supratransmission, consists in a sudden decrease in the amplitude of wave signals of a medium which is already locked in the conducting regime, when the driving amplitude is decreased under a critical value: The *infratransmission threshold*.

In the present work, we show that a medium governed by a damped, spatially continuous, double sine-Gordon equation exhibits the presence of both nonlinear supratransmission and infratransmission. As a corollary, double sine-Gordon media may exhibit the presence of nonlinear bistability. Our simulations will be based on an extension for continuous media of the numerical method presented in Ref. 16. Moreover, the computational technique employed in our present manuscript will approximate the dynamics of a general class of nonlinear partial differential equations of the hyperbolic type with arbitrary potential functions. As expected, the technique will not only approximate consistently the solutions to the initial-boundary-value problem under consideration, but it will also approximate the local energy density, the total energy of the system, the total energy accumulated throughout time; in addition, it will preserve the nonnegative character of the local energy and the total energy operators of the continuous case scenario. As we will see in this work, the nonlinear phenomena of supratransmission and infratransmission will allow us to modulate the perturbation on the driving boundary of the medium under study, in such way that monochromatic waves will be transmitted into the system in a reliable and accurate fashion.

In our investigation, we have included the presence of damping for two main reasons: Firstly, physically realistic models necessarily reflect the presence of damping in one way or another. Secondly, even when the process of supratransmission is present in several damped or undamped media [8-12], some of those works show that, once that the medium has reached the conducting regime, infratransmission demands the presence of damping in order for the system to stop absorbing energy when the driving amplitude decreases drastically [11]. As we will see, the process of bistability in our work will be characterized mathematically by the presence of bilinear soliton solutions for the system under investigation and, physically, by the coalescence of a conducting and an insulating regimes.

Our work is sectioned in the following way: In Sec. 2, we introduce the initial-boundary-value problem that motivates our study, together with the associated local energy density, the total energy of the system, and the total energy accumulated over a finite interval of time. Section 3 introduces the numerical method employed to approximate the solution of the problem under investigation. Here, we present the finite-difference schemes used to approximate the solution to the problem, the local energy density, the total energy of the system at any time, and the accumulated energy over temporal intervals, followed by some remarks on the computational implementation of our technique. Section 4 is devoted to show simulations that support the existence of the process of nonlinear bistability in the problem under study. In turn, Sec. 5 presents two applications of the phenomenon of bistability to the propagation of monochromatic waves in the medium of interest. Here, we show that supratransmission and infratransmission may be employed in two different forms, in order to propagate information in an accurate and efficient way in media governed by damped, double sine-Gordon equations. Finally, we close our study with a section of concluding remarks and directions of further investigation.

2. Preliminaries

2.1. Mathematical model

Let D be a spatial interval of the form $[0, L] \subset \mathbb{R}$, and let $\mathbb{R}^+$ represent the set of nonnegative real numbers. Let t represent time, and assume that u is a function of the ordered pair (x, t), where $x \in D$ and $t \in \mathbb{R}^+$. Moreover, let γ be a nonnegative real number. In this work, we investigate the dynamics of the initial-boundary-value problem

$$\frac{\partial^2 u}{\partial t^2} - \frac{\partial^2 u}{\partial x^2} + \gamma \frac{\partial u}{\partial t} + G'(u) = 0, \quad (x,t) \in D \times \mathbb{R}^+,$$

$$\text{s.t.} \begin{cases} \dfrac{\partial u}{\partial t}(x,0) = u(x,0) = 0, & x \in D, \\ u(0,t) = A\sin(\Omega t), & t \geq 0, \\ \dfrac{\partial u}{\partial x}(L,t) = 0, & t \geq 0. \end{cases} \tag{1}$$

From a physical perspective, it is clear that the constant γ represents the coefficient of external damping of the system. Moreover, for our simulations, we will fix a potential function of the form

$$G(u) = \frac{1}{6}\left[2 - 2\cos u - \cos(2u)\right], \tag{2}$$

whence the double sine-Gordon law

$$G'(u) = \frac{1}{3}\left[\sin u + \sin(2u)\right] \tag{3}$$

readily results. A system governed by (1) is, in general, dissipative, and it is not difficult to show that the Hamiltonian density associated to the conservative version (to be more precise, when no damping is present) of the nonlinear, hyperbolic partial differential equation in (1), is the function $H : D \times \mathbb{R}^+ \to \mathbb{R}$ given by

$$H(x,t) = \frac{1}{2}\left(\frac{\partial u}{\partial t}\right)^2 + \frac{1}{2}\left(\frac{\partial u}{\partial x}\right)^2 + G(u), \qquad (4)$$

which results from the Lagrangian $\mathcal{L} : D \times \mathbb{R}^+ \to \mathbb{R}$ provided by the expression

$$\mathcal{L}(x,t) = \frac{1}{2}\left(\frac{\partial u}{\partial t}\right)^2 - \frac{1}{2}\left(\frac{\partial u}{\partial x}\right)^2 - G(u). \qquad (5)$$

Here, the dependency of u on (x,t) is obviated for the sake of simplicity. The total energy of the system at time t is provided by the expression

$$E(t) = \int_0^L H(x,t)\,dx. \qquad (6)$$

Meanwhile, for every positive, real number T, the total energy accumulated by the system over a finite interval of time $[0,T]$ is given by

$$\mathcal{E}_T = \int_0^T E(t)dt. \qquad (7)$$

It is important to notice that the local energy density (4), the total energy of the medium (6) and the accumulated energy (7), are all nonnegative operators. Moreover, our physical model satisfies the following mathematical identity.

Proposition 1. *The functional $E(t)$ associated to the partial differential equation in* (1) *satisfies*

$$\frac{dE}{dt} = \left(\frac{\partial u}{\partial t}\frac{\partial u}{\partial x}\right)\Big|_{x=0}^{x=L} - \gamma\int_0^L \left(\frac{\partial u}{\partial t}\right)^2 dx. \qquad (8)$$

Proof. The proof is straightforward. □

Proposition 1 is important for numerical considerations on the stability and the multi-domain consistency of the method presented in the following section. Of course, a convenient reduction of (8) is readily at hand if we take into account the Dirichlet datum on the left end of D, and the homogeneous Neumann condition imposed on the right. As a corollary, the energy of (1) is preserved throughout time in the undamped scenario when either fixed Dirichlet boundary data or homogeneous Neumann boundary conditions are imposed.

Remark 2. The multiplicative constant $1/3$ in the expressions of (2) and (3) has been included for the sake of convenience. As we will show in the next step of our study, the inclusion of such constant yields a normalized expression of the forbidden band-gap region associated to the linear mode solutions of the linearized form of the partial differential equation in (1). □

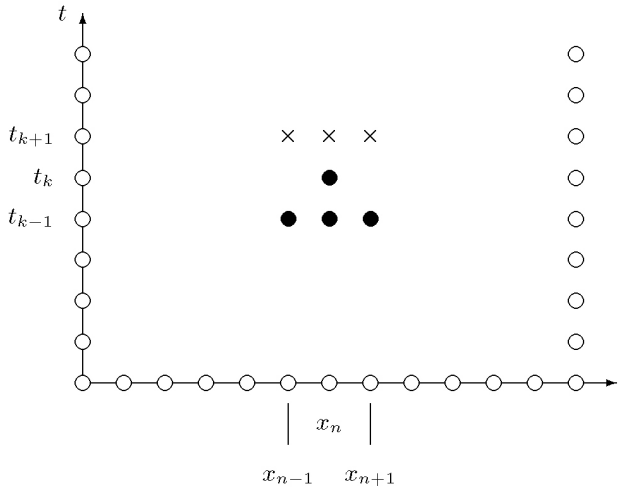

FIGURE 1. Forward-difference stencil for the approximation to the solution of the initial-boundary-value problem (1) at time t_k, using the numerical method (19). The black circles represent known approximations to the actual solutions at the times t_{k-1} and t_k, and the crosses denote the unknown approximations at the time t_{k+1}.

2.2. Forbidden band-gap

Let γ be equal to zero. Linearizing the partial differential equation of (1), we obtain the equation

$$\frac{\partial^2 u}{\partial t^2} - \frac{\partial^2 u}{\partial x^2} + u = 0, \quad (x,t) \in D \times \mathbb{R}^+. \qquad (9)$$

We consider linear mode solutions of (9) of the form $u(x,t) = A_0 e^{i(kx-\omega t)}$, where the wave frequency ω depends on the wave number k. A straight-forward substitution yields the linear dispersion relation

$$\omega^2(k) = k^2 + 1. \qquad (10)$$

In the investigation of the nonlinear processes of supratransmission and infratransmission below, we will restrict our attention to the forbidden band-gap region $\Omega < 1$ associated to (10).

3. Computational technique

3.1. Finite-difference scheme

Suppose that T is a positive real number. Let $0 = x_0 < x_1 < \ldots < x_N = L$ be a regular partition of the spatial interval D with norm equal to Δx, and let $0 = t_0 < t_1 < \ldots < t_M = T$ be a regular partition of the temporal interval $[0,T]$ with norm equal to Δt (obviously, $\Delta x = (b-a)/N$ and $\Delta t = T/M$). For every $k = 0, 1, \ldots, M$ and every $n = 0, 1, \ldots, N$, let

$$\phi_k = A\sin(\Omega t_k), \qquad (11)$$

and let u_n^k be the approximation provided by the method to the actual solution of the problem (1) at the point x_n and the time t_k, that is, assume that $u_n^k \approx u(x_n, t_k)$.

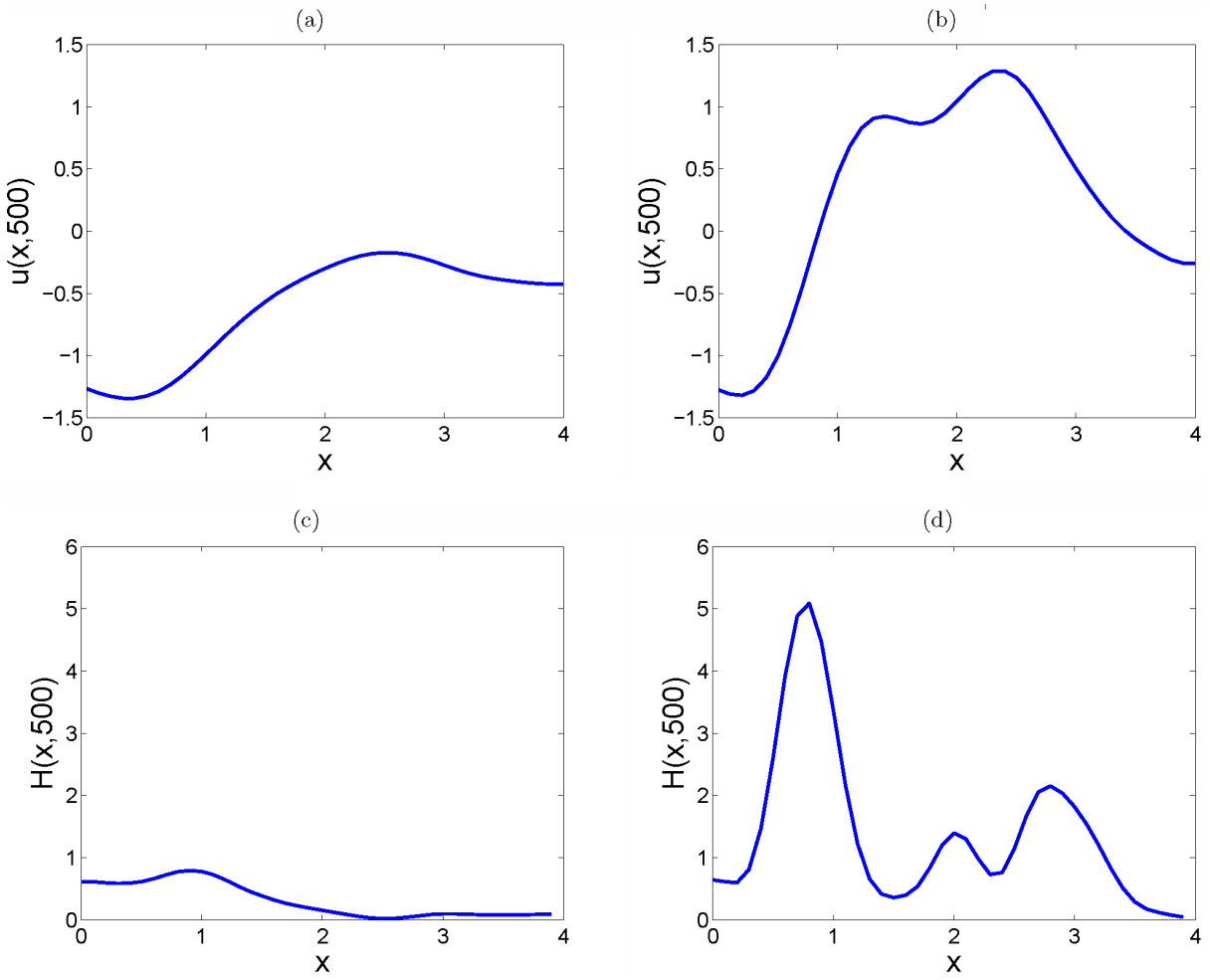

FIGURE 2. Approximate solution and approximate local energy density of the undamped, initial-boundary-value problem (1) at time 500 for the double sine-Gordon potential (2), spatially defined on $[0, 4]$, harmonically perturbed at the boundary at a frequency equal to 0.7, and two different driving amplitudes: 1.32 (left column) and 1.33 (right column). The top row presents the simulations corresponding to the solution of the problem, while the bottom row provides the numerical results corresponding to the local energy density. The total energy accumulated over the period of time is equal to 534.14 for $A = 1.32$, and 1719.7 for $A = 1.33$.

We introduce the standard, linear operators

$$\delta_t u_n^k = \frac{u_n^{k+1} - u_n^k}{\Delta t}, \tag{12}$$

$$\delta_t^{(1)} u_n^k = \frac{u_n^{k+1} - u_n^{k-1}}{2\Delta t}, \tag{13}$$

$$\delta_t^{(2)} u_n^k = \frac{u_n^{k+1} - 2u_n^k + u_n^{k-1}}{(\Delta t)^2}, \tag{14}$$

which are used to approximate the first-order partial derivative of u with respect to t in the first two cases, and the second-order partial derivative of u with respect to t in the last. We also employ the linear operator

$$\delta_x^{(2)} u_n^k = \frac{u_{n+1}^k - 2u_n^k + u_{n-1}^k}{(\Delta x)^2}, \tag{15}$$

in order to approximate the second-order partial derivative of u with respect to x, with a consistency of the second order in space. Evidently, the operator (12) is a first-order, temporal approximation of the partial derivative of u with respect to t at (x_n, t_k), and (13) is a second-order estimate of the same value. Meanwhile, (14) is an approximation of the second-order partial derivative of u with respect to t, with a consistency of the second order in time.

Likewise, we introduce the temporal average operator

$$\mu_t^{(1)} u_n^k = \frac{1}{2}\left(u_n^{k+1} + u_n^{k-1}\right), \tag{16}$$

which is consistent of the second order in time with the exact value of u at (x_n, t_k). We also introduce the discrete derivative of G with respect to u and the time average of G at u, respectively, as the discrete operators

$$\delta_u^{(1)} G(u_n^k) = \frac{G(u_n^{k+1}) - G(u_n^{k-1})}{u_n^{k+1} - u_n^{k-1}}, \tag{17}$$

$$\mu_t G(u_n^k) = \frac{G(u_n^{k+1}) + G(u_n^k)}{2}. \tag{18}$$

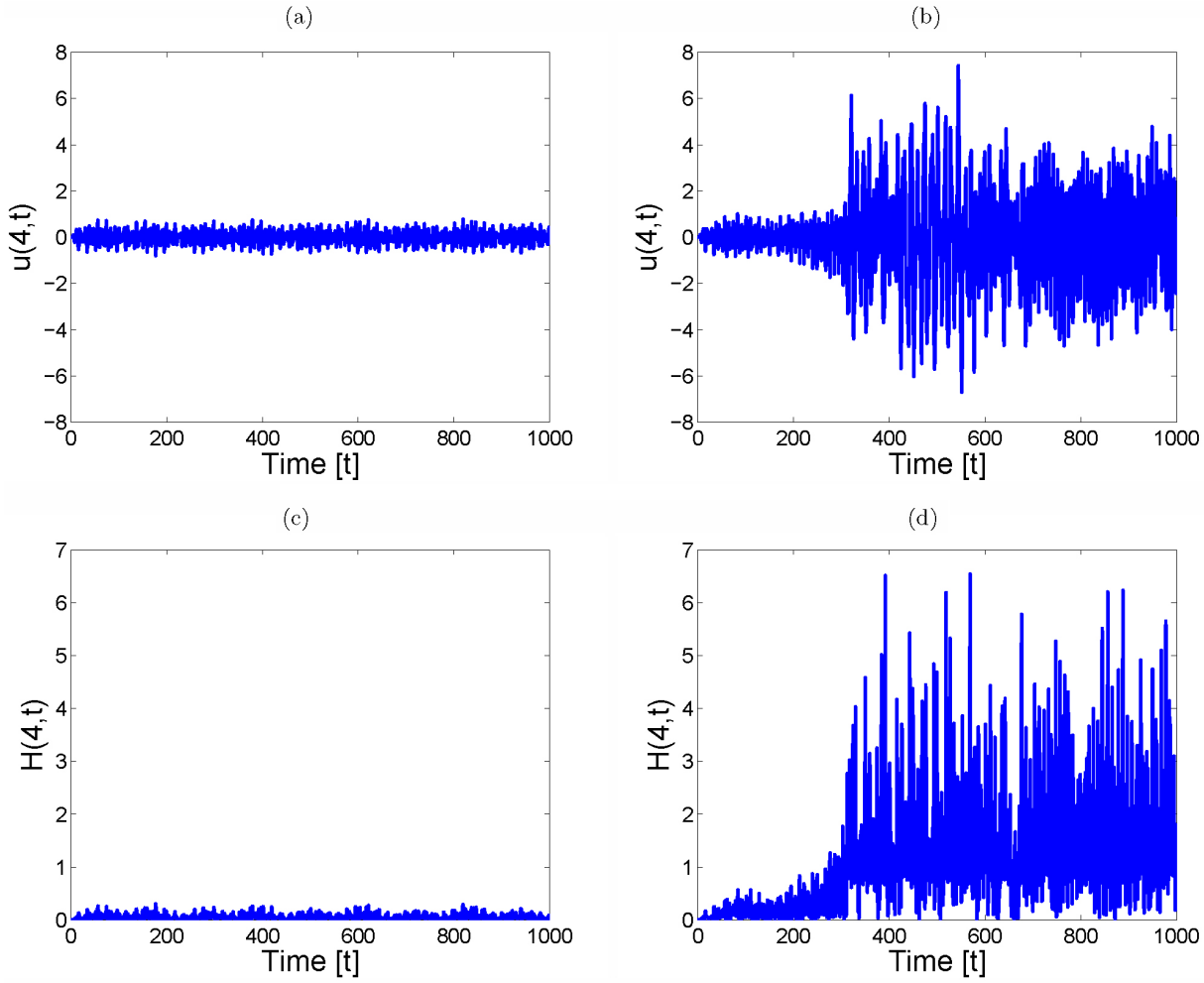

FIGURE 3. Dynamics of the approximate solution and the approximate local energy density of the undamped, initial-boundary-value problem (1) at $x = 4$ with double sine-Gordon potential (2), harmonically perturbed at the boundary at a frequency equal to 0.7, and two different driving amplitudes: 1.32 (left column) and 1.33 (right column). The top row presents the simulations corresponding to the solution of the problem, while the bottom row provides the numerical results corresponding to the local energy density. The problem is spatially defined on the interval $[0, 4]$, and temporally on $[0, 1000]$

Under these circumstances, the numerical method used in this work to approximate the solution to the initial-boundary-value problem (1) is given by

$$\delta_t^{(2)} u_n^k - \mu_t^{(1)} \delta_x^{(2)} u_n^k + \gamma \delta_t^{(1)} u_n^k + \delta_u^{(1)} G(u_n^k) = 0,$$

$$\begin{cases} u_n^0 = u_n^1 = 0, & n = 0, 1, \ldots, N, \\ u_0^k = \phi_k, & k = 0, 1, \ldots, M, \\ u_N^k - u_{N-1}^k = 0, & k = 0, 1, \ldots, M; \end{cases} \tag{19}$$

its forward-difference stencil is presented in Fig. 1. The discretized version of the energy density functional (4) is provided by the discrete operator

$$H_n^k = \frac{1}{2} \left[\left(\delta_t u_n^k \right)^2 + \sum_{j=n-1}^{n} \sum_{l=k}^{k+1} \frac{\left(\delta_x u_j^l \right)^2}{4} \right] + \mu_t G(u_n^k), \tag{20}$$

and the total energy of the system at time t_k is approximated by the expression

$$E^k = \sum_{n=1}^{N-1} H_n^k \, \Delta x + \frac{1}{2} \sum_{l=k}^{k+1} \frac{\left(\delta_x u_0^l \right)^2}{4} \Delta x. \tag{21}$$

Evidently, the total energy of the system accumulated over the temporal interval $[0, T]$ will be approximated by

$$\hat{\mathcal{E}}_T = \sum_{k=1}^{M} E^k \Delta t. \tag{22}$$

From a computational point of view, the finite-difference method (19) provides approximations to the solutions of the partial differential equation in (1) which, in the linear regime, are consistent estimations of order $\mathcal{O}((\Delta t)^2 + (\Delta x)^2)$. Additionally, it is clear that the discrete operators (20) and (21) yield consistent approximations of the first order to (4) and (6), respectively.

The following is the discrete version of Proposition 1. It shows that the consistency of our method is also preserved

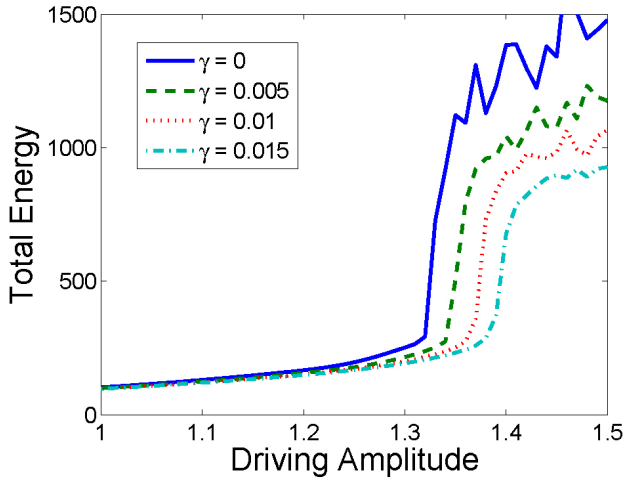

FIGURE 4. Graph of the accumulated total energy over the temporal interval $[0, 300]$ versus driving amplitude, of a system governed by problem (1) on the spatial domain $[0, 4]$. The driving frequency is equal to 0.7, the potential function G is provided by (2), the driving amplitude takes on values in $[1, 1.5]$, and four different damping coefficients were employed, namely, 0 (solid), 0.005 (dashed), 0.01 (dotted) and 0.015 (dashed-dotted).

on the grounds of the energy domain when the medium is conservative.

Proposition 3. *Consider the finite-difference scheme* (19)*, with local energy given by* (20)*, and total energy* (21)*. Then, the following identity is satisfied at the* $(k-1)$*st time-step:*

$$\delta_t E^{k-1} = -\left(\mu_t^{(1)}\delta_x u_0^k\right)\left(\delta_t^{(1)}u_0^k\right) - \gamma\sum_{n=1}^{N-1}\left(\delta_t^{(1)}u_n^k\right)^2 \quad (23)$$

Proof The proof is a direct consequence of mere, algebraic manipulations of the expressions (19), (20) and (21).

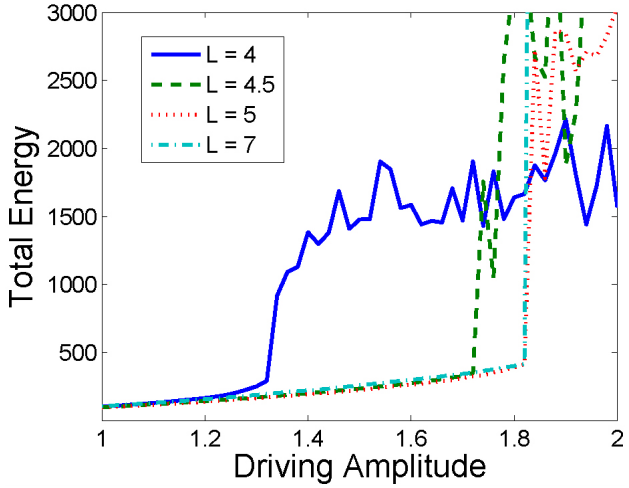

FIGURE 5. Graph of the accumulated total energy over the temporal interval $[0, 300]$ versus driving amplitude, of an undamped system governed by problem (1) on the spatial domain $[0, L]$. The driving frequency is equal to 0.7, the potential function G is provided by (2), and four different lengths L were employed, namely, 4 (solid), 4.5 (dashed), 5 (dotted) and 7 (dashed-dotted). The driving amplitude takes on values in $[1, 2]$.

3.2. Computational remarks

Throughout this section, we follow the nomenclature employed in the previous stage.

To start off, it is important to point out that the local energy function given by (4) is nonnegative for the double sine-Gordon regime investigated here; evidently, its discrete counterpart, namely, the operator (20), is likewise nonnegative. It follows that the total energy of the medium as given by (6), as well as the discrete total energy (21), are both nonnegative at any time. Moreover, the total energy of the medium over finite periods of time (7), along with its discrete approximation (22), are also nonnegative functionals.

On the other hand, the finite-difference scheme (19) is nonlinear and implicit when G is not a constant function, as it is the case with the double sine-Gordon chain. Thus, in order to approximate the solution of the regime (1) at time t_{k+1} when the approximations at times t_k and t_{k-1} are at hand, we employ Newton's method for nonlinear systems of equations. More accurately, for every $k \in \{0, 1, \ldots, M\}$, let $\mathbf{u}^k = (u_0^k, u_1^k, \ldots, u_N^k)$. Let f_n be the left-hand side of the nth difference equation of (19), that is, let

$$f_n(\mathbf{u}^k) = \delta_t^{(2)}u_n^k - \mu_t^{(1)}\delta_x^{(2)}u_n^k + \gamma\delta_t^{(1)}u_n^k + \delta_u^{(1)}G(u_n^k), \quad (24)$$

for every $n \in \{1, \ldots, N-1\}$. Additionally, let

$$f_0(\mathbf{u}^k) = u_0^k - \phi_k, \quad (25)$$

$$f_N(\mathbf{u}^k) = u_N^k - u_{N-1}^k, \quad (26)$$

and let $\mathbf{f} = (f_0, f_1, \ldots, f_N)$. Using a recursive process, assume that the vectors $\mathbf{u}^k$ and $\mathbf{u}^{k-1}$ have been previously computed. One readily checks that

$$\mathbf{u}^{k+1} = \mathbf{u}^k - \mathbf{y}, \quad (27)$$

where $\mathbf{y}$ is the $(N+1)$-dimensional, real vector which satisfies the matrix equation

$$J(\mathbf{u}^k)\mathbf{y} = -\mathbf{f}(\mathbf{u}^k). \quad (28)$$

Evidently, the matrix J is the Jacobian matrix of $\mathbf{f}$, which is given by

$$J(\mathbf{u}^k) = \begin{pmatrix} 1 & 0 & 0 & 0 & \cdots & 0 & 0 & 0 \\ a & d_1 & a & 0 & \cdots & 0 & 0 & 0 \\ 0 & a & d_2 & a & \cdots & 0 & 0 & 0 \\ \vdots & \vdots & \vdots & \vdots & \ddots & \vdots & \vdots & \vdots \\ 0 & 0 & 0 & 0 & \cdots & a & d_{N-1} & a \\ 0 & 0 & 0 & 0 & \cdots & 0 & -1 & 1 \end{pmatrix}. \quad (29)$$

Here

$$a = -\frac{1}{2(\Delta x)^2}, \quad (30)$$

$$d_n = \frac{1}{(\Delta t)^2} + \frac{1}{(\Delta x)^2} + \frac{\gamma}{2\Delta t} + \frac{\left(u_n^{k+1} - u_n^{k-1}\right)G'(u_n^{k+1}) + G(u_n^{k-1}) - G(u_n^{k+1})}{\left(u_n^{k+1} - u_n^{k-1}\right)^2}, \quad (31)$$

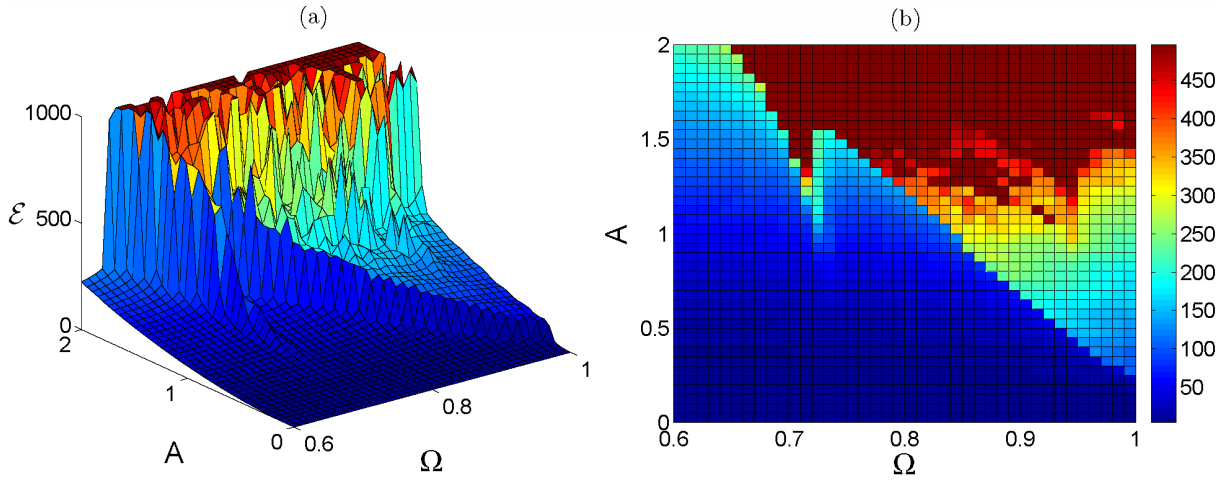

FIGURE 6. Graph (a) shows the accumulated total energy $\mathcal{E} = \mathcal{E}_{300}$ over the temporal interval $[0, 300]$ versus driving frequency and driving amplitude of a system governed by (1) spatially defined on $[0, 4]$, with constant damping coefficient equal to 0.005 and potential function provided by (2). The right column shows the corresponding check-plot graph. In both instances, the driving frequency and the driving amplitude take on values in the intervals $[0.6, 1]$ and $[0, 2]$, respectively.

for every $n \in \{1, \ldots, N-1\}$. The tridiagonal system (28) is solved then employing Crout's reduction technique with pivoting [21], in order to reduce the computer propagation of rounding errors.

4. Nonlinear bistability

Throughout this section, we study the system (1) for the double sine-Gordon potential (2). It is known that the spatially discrete version of this model presents the phenomenon of nonlinear supratransmission [9], for driving frequencies in the forbidden band-gap region $\Omega < 1$. In the present stage, we follow a standard methodology (see [8]) in order to establish that this process is also present in the spatially continuous problem (1).

4.1. Supratransmission

Consider the undamped form of the initial-boundary-value problem (1), spatially defined on [0,4], and fix a driving frequency equal to 0.7. Two driving amplitudes are considered, namely, 1.32 and 1.33. Under these circumstances, the top row of Fig. 2 presents the solution of our problem for $A = 1.32$ (left) and $A = 1.33$ (right), at time 500. Seemingly, there is a qualitative difference in both simulations: while the smaller amplitude does not result in the propagation of wave fronts into the medium, the greater amplitude does. To confirm this observation, the bottom row of Fig. 2 presents the energy density of the problem at time 500, for the two driving amplitudes considered. The left graph shows the local energy density corresponding to $A = 1.32$ and, compared to the right graph (which corresponds to a driving amplitude equal to 1.33), it is relatively smaller. This comparison evidently shows a difference between the qualitative behavior of the dynamics of the system around the critical amplitude $A = 1.32$. Moreover, the total energy over the temporal period [0,500] for the smaller amplitude is equal to 534.14, while the accumulated energy in the second case is equal to 1719.7.

In order to confirm the presence of the process of nonlinear supratransmission in the medium under investigation, we have computed the temporal behavior of the solution and the local energy around $x = 4$, for the system described in the previous paragraph. The dynamics of the solution at this point is presented as the top row of Fig. 3 for the two amplitudes considered before, over the temporal interval [0,1000]. The solution for $A = 1.32$ (left column) oscillates relatively close to the value of 0, while the solution corresponding to $A = 1.33$ (right column) exhibits oscillations of higher amplitude after the time $t = 250$. This drastic change in the behavior of the medium is also found in the domain of the local energy, as the bottom row of the same graph shows. The presence of the process of nonlinear supratransmission is thus suggested by our computations, and we will corroborate it in the next calculations following a standard methodology [16].

Remark 4. Before we proceed to present more numerical evidence in favor of the presence of the process of nonlinear supratransmission in (1), we must point out that the soliton solutions depicted in Fig. 2(a) and (b) move from the driving boundary to the right at approximately the same constant speed. When the system is in the insulating regime, the wave moves as a pulse with low (though non-constant) amplitude; meanwhile, the wave is a moving breather with higher (non-constant) amplitude when the medium is locked in the conducting regime. The pattern shown in the figure is repeated at relatively regular intervals of time, that is, localized nonlinear modes are created at approximately fixed temporal periods. These assertions are also true in the case when damping is present; however, in this situation, the amplitude of the wave signals decreases as the solitons move away from the origin.

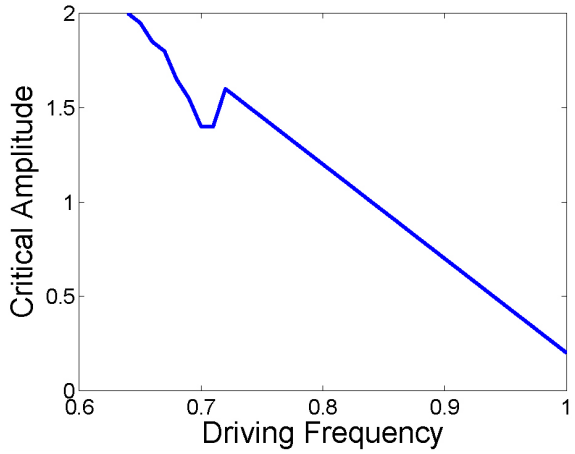

FIGURE 7. Graph of critical amplitude at which supratransmission starts versus driving frequency, of a system governed by (1) spatially defined on $[0, 4]$, with constant damping coefficient equal to 0.005 and potential function provided by (2). The graph was obtained using the information presented in Fig. 6. Here, the driving frequency and the driving amplitude take on values in the intervals $[0.6, 1]$ and $[0, 2]$, respectively.

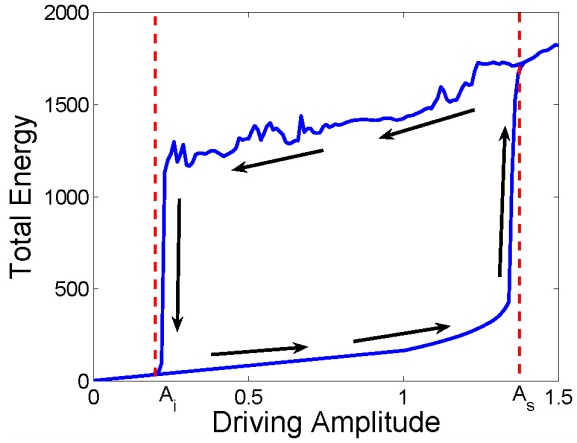

FIGURE 8. Graph of the total energy accumulated over a temporal period of length 500 versus driving amplitude, of a medium governed by (1) spatially defined on $[0, 4]$, with damping coefficient equal to 0.005 and driving frequency equal to 0.7. The portion of the graph corresponding to the arrows pointing right represents the energy of a medium which was initially at rest with initial driving amplitude equal to 0, while the arrows pointing left correspond to a system whose initial conditions are those of a conducting regime with initial driving amplitude equal to the supratransmission threshold. The driving amplitudes take on values in the interval $[0, 1.5]$.

Let us consider again the initial-boundary-value problem (1) spatially defined on the interval [0,4], subject to a driving frequency equal to 0.7. We approximate now the total energy accumulated over the temporal interval [0,300], for several damping coefficients and several driving amplitudes. The results are presented as Fig. 4, for values of the driving amplitude within [1,1.5], and values of γ equal to 0, 0.005, 0.01 and 0.015. In each case, an abrupt increase in the energy absorbed by the system through the driving boundary is observed above some critical value A_s which depends on γ.

Naturally, it is important to check the presence and the behavior of the critical amplitude A_s for different interval lengths. So, consider the medium (1) with no damping, subject to a driving frequency of 0.7 on the left end of the spatial interval [0,L], and compute the total energy over the temporal interval [0,300], for driving amplitudes in the set [1,2]. Under these conditions, Fig. 5 presents the amplitude-dependence of the total energy accumulated by the medium over the given temporal period, for various values of L, namely, 4, 4.5, 5 and 7. In these four cases, the system exhibits the presence of the phenomenon of nonlinear supratransmission. Moreover, our simulations indicate that the critical amplitude at which supratransmission occurs tends to a fixed real number around 1.83 as L is increased.

We have conducted computational experiments in order to establish the existence of a critical amplitude A_s at which supratransmission starts, for several driving frequencies in the forbidden band-gap region $\Omega < 1$. To that effect, we fixed regular partitions of the frequency interval [0.6,1] and the amplitude interval [0,2] and, for each such frequency and amplitude, we computed the accumulated energy over the temporal interval [0,300]. The results of our simulations are summarized in Fig. 6(a) as a graph of total energy over the given period of time versus driving frequency and driving amplitude and as an interpolated check-plot graph in Fig. 6(b), for a system governed by (1) with damping coefficient equal to 0.005, spatially defined on [0,4]. The result shows that the accumulated energy blows up above a critical driving amplitude which depends on the driving frequency. This phenomenon is identified as *nonlinear supratransmission*, and its occurrence is prescribed in Fig. 7 for the system under study, as a bifurcation diagram of the critical amplitude at which nonlinear supratransmission occurs versus driving frequency.

Remarks 5.

(a) Observe that the results presented so far correspond to an idealistic system in which damping is not present. In a more realistic situation, the value of the parameter γ is not equal to zero and, as we shall see in the next sections, the phenomenon of nonlinear supratransmission is also present in such cases. However, we deemed convenient to include this preliminary approach in order to show that supratransmission is not exclusive of damped, double sine-Gordon chains.

(b) Also, we must point out that we have detected the presence of supratransmission in relatively long arrays governed by (1). As far as the author knows, this fact has not been established analytically for double sine-Gordon equations. However, the presence of this nonlinear process has been proved in the (bounded or semi-unbounded) undamped Frenkel-Kontorova model, using the fact that the limiting medium becomes the classical sine-Gordon equation [11,12]. Similarly, the process has been analytically predicted and approximated in the undamped, classical β-Fermi-Pasta-Ulam chain [10].

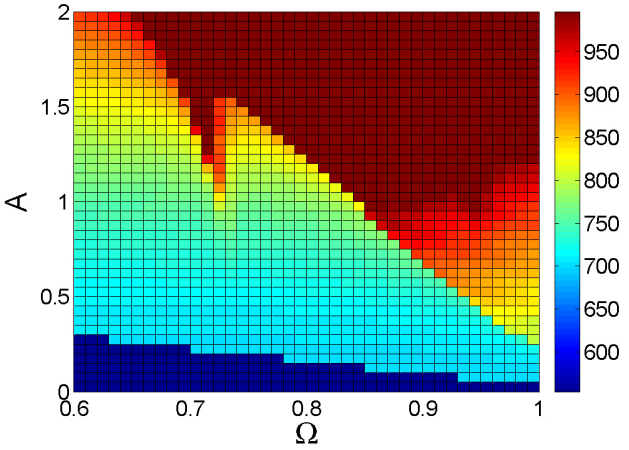

FIGURE 9. Check-plot graph of the total energy accumulated over a temporal period of 500 versus driving frequency and driving amplitude of a system governed by (1) spatially defined on $[0, 4]$, with constant damping coefficient equal to 0.005 and potential function provided by (2). The these results represent the sum of the check-plot in Fig. 6, and the corresponding infratransmission curve plotted in Fig. 8, now for several driving frequencies in the interval $[0.6, 1]$ and amplitudes in the set $[0, 2]$.

4.2. Infratransmission

We want to establish now the presence of the process of infratransmission in (1). To that effect, we consider a medium which has already reached the conducting regime. More concretely, we study a system governed by (1) spatially defined on the interval [0,4], with potential function (2) and damping coefficient equal to 0.005. A driving frequency equal to 0.7 is fixed, for which the supratransmission threshold is equal to 1.35. The driving amplitude is varied in the interval [0,1.5] and, for each such value, the total energy accumulated over a period of time of 500 is recorded, until the supratransmission threshold is found. Next, taking as initial conditions those of a system which is already in a conducting state with driving amplitude equal to the supratransmission threshold, we slowly decrease the value of the amplitude and, for each amplitude value, we record the total energy of the system over a temporal period of 500, until the medium locks itself into an insulating regime.

The results of our simulations are presented as a hysteresis diagram in Fig. 8, where the direction of the arrows indicates the direction of increase or decrease of the amplitude. The results evidence the existence of the infratransmission threshold and, ultimately, of a bistable regime in the double sine-Gordon system. In this graph, the infratransmission threshold is approximately equal to 0.19, while the supratransmission threshold is approximately equal to 1.36, a value which is in good qualitative agreement with the results displayed in Fig. 4.

We must declare that we have performed more simulations for different values of the parameters γ and Ω (with $0 \leq \gamma \ll 1$ and Ω in the forbidden band-gap), and that we have found the presence of nonlinear bistability in all of them.

The results of our computations for a damping coefficient equal to 0.005 are presented in Fig. 9 in the form of a check-plot graph of total energy over the temporal interval [0,300] versus driving amplitude and driving frequency, following the methodology employed to obtain the *infratransmission function* in Fig. 8, that is, the function which has associated arrows pointing left. More accurately, we added the function pictured in Fig. 6(b) and the corresponding infratransmission check-plot (not pictured here for the sake of briefness), the result being Fig. 9. As a consequence, an important conclusion of this investigation is the discovery of the nonlinear processes of supratransmission and infratransmission and, ultimately, the presence of a nonlinear bistable regime in the $(1 + 1)$-dimensional, double sine-Gordon equation.

5. Wave propagation

Let Ω be a frequency in the forbidden band-gap region of (1). Fix a particular value of the damping coefficient and, for each fixed pair of parameters (Ω, γ), let A_i and A_s be, respectively, the infratransmission and the supratransmission thresholds of the medium. Evidently, $A_i < A_s$. The purpose of this section is to show that two different perturbation techniques based on the modulation of the driving amplitude of (1) may be used to transmit binary information from the left boundary of D to the right end.

5.1. First method

Fix a spatial domain D, and let n be a positive integer number. Assume that $\mathbf{b} = (b_1, \ldots, b_n)$ is a finite sequence of length n consisting of zeros and ones, and let b_0 be equal to 0. We will modulate the amplitude of the harmonic perturbation on the left boundary of D, in order to transmit the binary information contained in $\mathbf{b}$ to the free boundary. So, let P be a positive, real number which physically represents the period during which a binary bit will be generated at the perturbed boundary and propagated into the medium. For our simulations P will be relatively much greater than 100.

For every integer number j, let I_j be the interval $[j-1, j]$. Let $B_j = (1 - b_j)A_i + b_j A_s$, for every $j \in \{0, 1, \ldots, n\}$. We consider a system governed by (1), with time normalized with respect to the value of P. The initial instant of time will be reset to -1 for practical purposes. The amplitude $A(t)$ of the perturbation at the left end of D is linearly increased from 0 to the value A_i during the first $100/P$ units of the interval I_0; for the rest of this temporal interval, the amplitude will be constant and equal to A_i. Recursively, assume that the driving function has been defined in the interval I_{j-1}, for some $j \in \{1, \ldots, n\}$. We linearly change the value of $A(t)$ from B_{j-1} to B_j during the first $100/P$ units of time of I_j, and we let $A(t)$ be equal to B_j for the rest of the values of $t \in I_j$. More precisely, we let

$$A(t) = \begin{cases} \inf\left\{\dfrac{PB_0}{100}(t+1), B_0\right\}, & t \in I_0, \\ \operatorname{mid}\left(B_{j-1}, A_j(t), B_j\right), & t \in I_j, \end{cases} \tag{32}$$

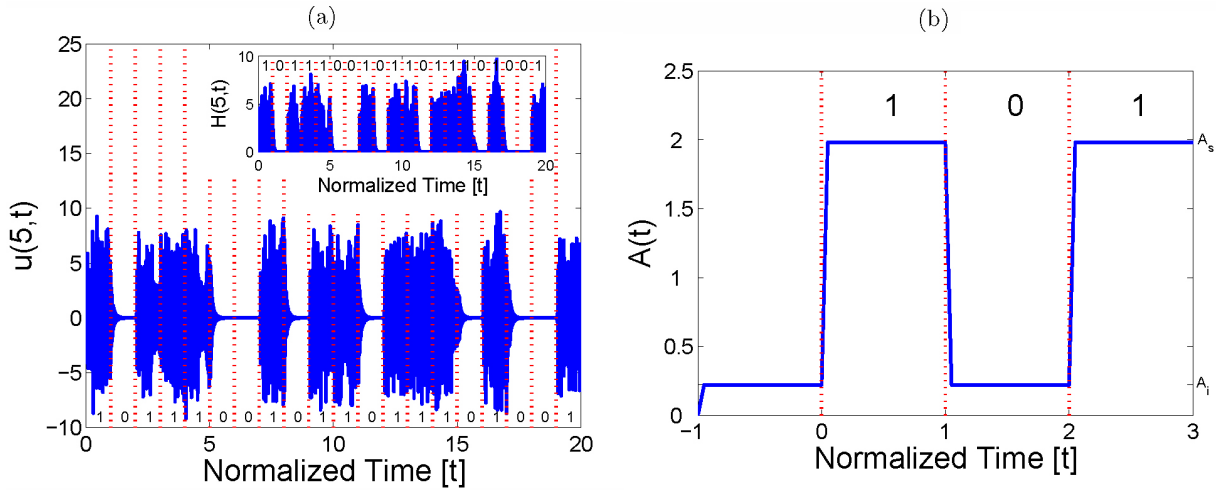

FIGURE 10. (a) Graph of the solution u at the point $x = 5$ of a system governed by (1) versus normalized time, with a damping coefficient equal to 0.01 and spatially defined in the interval $[0, 5]$. The driving frequency is equal to 0.7, and the potential function G is provided by (2). The approximate critical thresholds are $A_i = 0.22$ and $A_s = 1.98$. The driving amplitude function is provided by (32) as a consequence of transmitting the binary sequence (35), with a period of normalization $P = 2000$. The inset is the corresponding graph of the local energy density H near $x = 5$ versus normalized time. (b) Partial graph of the corresponding function A versus normalized time t, as given by (32).

where $A_j : I_j \to \mathbb{R}$ is given by

$$A_j(t) = B_{j-1} + P\left(\frac{B_j - B_{j-1}}{100}\right)(t - j + 1) \qquad (33)$$

and, for every $x, y, z \in \mathbb{R}$, the function $\mathrm{mid} : \mathbb{R}^3 \to \mathbb{R}$ assigns the value in the middle of the set $\{x, y, z\}$ when these numbers are arranged in ascending (alternatively, descending) order, that is,

$$\mathrm{mid}(x, y, z) = \inf\{\sup\{x, y\}, \sup\{x, z\}, \sup\{y, z\}\}. \quad (34)$$

Example 6. Let us consider a spatial domain D of length 5, and use a damping coefficient equal to 0.01, for which the nonlinear infratransmission and supratransmission thresholds are approximately equal to 0.22 and 1.98, respectively. We fix the period P equal to 2000, and consider the binary sequence

$$\mathbf{b} = (1, 0, 1, 1, 1, 0, 0, 1, 0, 1, 1, 0, 1, 1, 1, 0, 1, 0, 0, 1) \quad (35)$$

With this conventions, Fig. 10(a) presents the dynamics of the solution of (1) at $x = 5$ with respect to the normalized time. Our results show that the periods when a bit equal to 1 is propagated into the medium correspond to perturbations of high amplitude at the left end of the spatial domain D; meanwhile, bits equal to 0 are reflected in the right end of D as perturbations of much smaller amplitude. This behavior is also seen in the domain of the local energy density near the point of interest, as the inset of Fig. 10(a) reveals. □

For illustration purposes, Fig. 10(b) shows a partial plot of the driving amplitude function A in (32) corresponding to the vector (35), versus the time normalized with respect to P. Particularly, it is interesting to notice that, in each interval I_j, the set $[j - 1, j - 1 + 100/P]$ is employed to linearly adjust the value of the driving amplitude of the system.

5.2. Second method

Assume again that the binary sequence $\mathbf{b} = (b_1, \ldots, b_n)$ is going to be transmitted from the left end of D to the free boundary, let P be again the period of time during which a single bit will be generated by the harmonically perturbed end, and let b_0 be equal to zero. Let ϵ and λ be two relatively small, positive real numbers, and consider the time normalized with respect to P. In this stage of our study, we will impose Dirichlet boundary conditions of the form

$$u(0, t) = [I(t) + S(t)]\cos(\Omega t) \qquad (36)$$

on the left end of the interval D, where

$$I(t) = \frac{1}{2}\left[(A_s - A_i)\sin(\lambda t) + A_i + A_s\right] \qquad (37)$$

and

$$S(t) = \epsilon \sum_{j=1}^{n} b_j \chi_{I_j}(t). \qquad (38)$$

Here, I_j represents the temporal interval $[j - 1, j)$ for each integer number j. Additionally, for every set $A \subseteq \mathbb{R}$, the function $\chi_A : \mathbb{R} \to \mathbb{R}$ is the *characteristic function* on A, which is equal to 1 in A, and zero otherwise.

The function $I(t)$ is called the *seed*, while the function $S(t)$ is called the *signal*. Clearly, if a bit equal to 1 appears in the jth position of the binary sequence $\mathbf{b}$, with $j \in \{1, \ldots, n\}$, then S is a constant function equal to ϵ over the temporal period I_j. On the other hand, if b_j is equal to zero, then S is identically equal to zero in that set. Also, we must mention that, in order to avoid the creation of shock waves around the initial time $t = -1$, we simulate an initial period of normalized time I_0 during which the function $I(t)+S(t)$ in (36) is multiplied by a coefficient which slowly and linearly increases from 0 to 1.

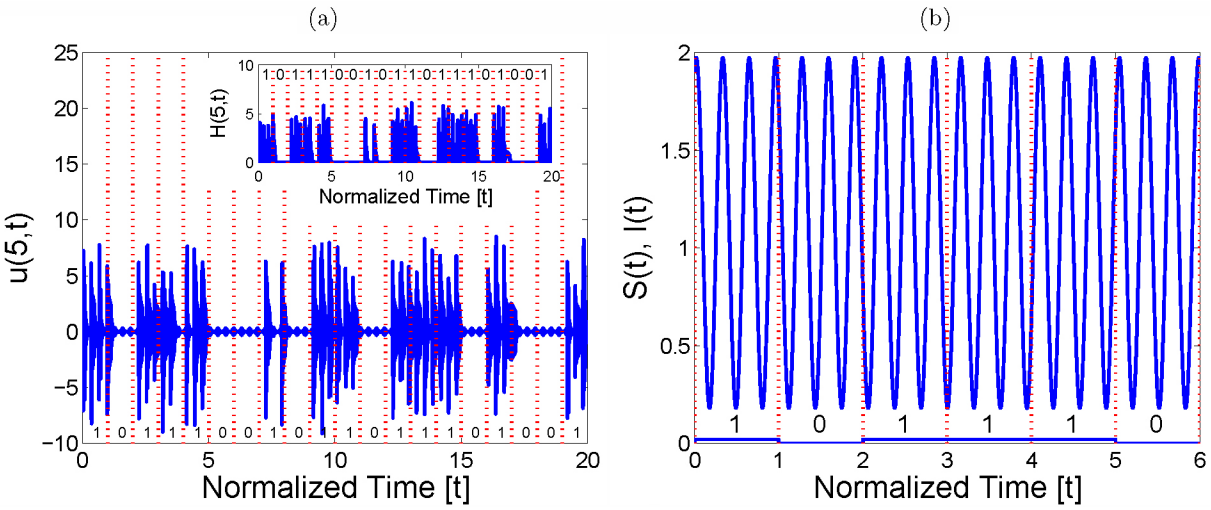

FIGURE 11. (a) Graph of the solution u at the point $x = 5$ of a system governed by (1) versus normalized time, with damping coefficient equal to 0.01 and spatially defined in the interval $[0, 5]$. The driving frequency is equal to 0.7, and the potential function G is provided by (2). The approximate critical thresholds employed are $A_i = 0.18$ and $A_s = 1.973$. The Dirichlet condition is provided by (36) as a consequence of transmitting the binary sequence (35), with a period of normalization $P = 4000$, $\lambda = 0.005$ and $\epsilon = 0.02$. The inset is the corresponding graph of the local energy density H near $x = 5$ versus normalized time. (b) Partial graph of the associated functions S and I versus normalized time t, as given by (37) and (38), respectively.

Remarks 7.

(a) Clearly, the seed represents a sinusoidal function which oscillates between the approximate infratransmission and supratransmission thresholds of the system.

(b) From a pragmatic perspective, the physical model (1) perturbed by the function (36) describes the temporal dynamics of a digital amplifier in which all the perturbations to be detected have the same amplitude ϵ, and are provided mathematically in the expression of the signal S.

(c) If one omits $I(t)$, the amplitude of the sinusoidal function (36) will be bounded within $[-\epsilon, \epsilon]$, a condition which does not even guarantee that the system will reach the excited regime at some point.

Remarks 8. Several considerations need to be made in order for (1) to work properly as a digital amplifier:

$\mathbf{C_1}$ The approximate critical values A_i and A_s must be slightly less than the exact thresholds of the system, which we denote here by A_i^* and A_s^*, respectively. More precisely,

$$0 < \max\{A_i^* - A_i, A_s^* - A_s\} < \epsilon. \qquad (39)$$

$\mathbf{C_2}$ In order for the system to modulate to the excited state, the length of each temporal interval I_j must be greater than the period of time that it takes for a localized nonlinear mode to be generated at the perturbed boundary.

$\mathbf{C_3}$ Additionally, each interval I_j must be sufficiently long in order for the system to be able to settle down into a non-excited regime.

$\mathbf{C_4}$ The wave length of the seed must be such that the function $I(t) + \epsilon - A_s^*$ be positive in temporal intervals sufficiently long in order to reach the supratransmission regime.

$\mathbf{C_5}$ Finally, the function $A_i^* - I(t)$ must be positive in intervals sufficiently long in order for the system to lock into the insulating regime.

Evidently, conditions $\mathbf{C_2}$ and $\mathbf{C_4}$ guarantee that the bit transition from 0 to 1 will result in the propagation of localized nonlinear modes into the system. In turn, $\mathbf{C_3}$ and $\mathbf{C_5}$ will cause the system to lock into a non-excited regime. These considerations are observed in the following example.

Example 9. Let P be equal to 4000, and let λ and ϵ be equal to 0.005 and 0.02, respectively. Fix the value of Ω equal to 0.7, let L be equal to 5, and consider a damping coefficient equal to 0.01, so that the approximate values of the infratransmission and the supratransmission thresholds are $A_i = 0.18$ and $A_s = 1.973$, respectively. We intend to transmit the binary sequence (35) from the left end of the spatial interval D to the right boundary by using the modulation function (36). The results of our simulations are displayed in Fig. 11(a), which shows the dynamical behavior of the solution at the right end of D, while the inset gives the corresponding graph of the local energy density. Evidently, the periods when a bit equal to 1 is transmitted correspond to temporal intervals of high activity in both domains, around the right boundary of

D, while the periods for bits equal to 0 correspond to periods of low activity.

For illustration purposes, Fig. 11(b) presents the graphs of the functions S and I for the first 6 periods of normalized time associated to the transmission of the binary sequence (35). One notices that the step function S is identically equal to zero during those periods associated to bits equal to 0, and it is equal to ϵ otherwise.

6. Conclusion

In this work, we established that a controlled propagation of localized modes in a sinusoidally perturbed, nonlinear medium governed by a double sine-Gordon equation with damping, is indeed feasible. In fact, we have established that binary information may be transmitted in a reliable way from one end of the spatial domain to the other, by modulating the amplitude of the transmitting end which, by the way, irradiates at a frequency in the forbidden band-gap. More concretely, we showed that our physical model exhibits the presence of the phenomena of nonlinear supratransmission and nonlinear infratransmission, and that the amplitude of the driving end may be modulated between the supratransmission and the infratransmission thresholds in order to transmit localized waves from the driving boundary.

As part of our study, we established the co-existence of a conducting and an insulating regimes in the double sine-Gordon model investigated. This discovery is in perfect agreement with similar qualitative results on discrete or continuous sine- and Klein-Gordon systems [8,11,12], and β-Fermi-Pasta-Ulam lattices [10]. The phenomenon is identified as the process of nonlinear bistability, which is a nonlinear phenomenon inherent to sine-Gordon, Klein-Gordon and β-Fermi-Pasta-Ulam regimes. We built hysteresis diagrams to evidence the presence of this process in our model and, moreover, we drew check-plot graphs and bifurcation diagrams to prescribe the occurrence of the nonlinear processes of supratransmission and infratransmission.

It must be mentioned in this point that our results rely on a numerical technique, in view that there is no general analytical apparatus to calculate the exact solutions of the problem under investigation. Our computational method, however, provides consistent approximations to the solutions of the hyperbolic partial differential equation studied in this work, and includes schemes to approximate the local energy density and the total energy of the system at any time, as well as a scheme to approximate the total energy accumulated by the medium over finite, temporal periods. Moreover, for a conservative system governed by (1), the computational technique is likewise conservative. This fact makes the method an ideal tool in the investigation of nonlinear supratransmission, which is better characterized in the energy domain.

Acknowledgments

The author would like to thank the anonymous reviewer for her/his invaluable comments which led to improve the overall quality of this work. The present manuscript reports on the final results of the research project PIM08-1 at the Universidad Autónoma de Aguascalientes, and is dedicated with profound devotion, deepest admiration and humble respect to colleague and co-author I.E. Medina-Ramírez.

1. M. Remoissenet, *Waves Called Solitons* 3rd ed. (Springer-Verlag, New York, 1999).
2. P.S. Lomdahl, O.H. Soerensen, and P.L. Christiansen, *Phys. Rev. B* **25** (1982) 5737.
3. C. Espinosa-Cerón, J. Fujioka, and R. F. Rodríguez, *Rev. Mex. Fis.* **52** (2006) 47.
4. J. Fujioka, E. Cabrera, and P.S. González-Pérez-Sandi, *Rev. Mex. Fis.* **53** (2007).
5. V.G. Makhankov, A.R. Bishop, and D.D. Holm, eds., *Nonlinear Evolution Equations and Dynamical Systems* Needs '94; Los Alamos, NM, USA 11-18 September '94: 10th International Workshop (World Scientific Pub. Co. Inc., Singapore, 1995), 1st ed.
6. J. Haro, *Rev. Mex. Fis.* **50** (2004).
7. A. Cruz-Osorio, A. González-Juárez, F.S. Guzmán, and F.D. Lora-Clavijo, *Rev. Mex. Fis.* **56** (2010) 456.
8. F. Geniet and J. Leon, *Phys. Rev. Lett.* **89** (2002) 134102.
9. F. Geniet and J. Leon, *J. Phys.: Condens. Matter* **15** (2003) 2933.
10. R. Khomeriki, S. Lepri, and S. Ruffo, *Phys. Rev. E* **70** (2004) 066626.
11. R. Khomeriki and J. Leon, *Phys. Rev. E* **71** (2005) 056620.
12. D. Chevriaux, R. Khomeriki, and J. Leon, *Phys. Rev. B* **73** (2006) 214516.
13. O.H. Olsen and M.R. Samuelsen, *Phys. Rev. B* **34** (1986) 3510.
14. D. Barday and M. Remoissenet, *Phys. Rev. B* **41** (1990) 10387.
15. Y.S. Kivshar, O.H. Olsen, and M.R. Samuelsen, *Phys. Lett. A* **68** (1992) 391.
16. J.E. Macías-Díaz, *Comput. Phys. Commun.* **181** (2010) 1842.
17. J. Leon and A. Spire, *Phys. Lett. A* **327** (2004) 474.
18. A.E. Kaplan, *Phys. Rev. Lett.* **55** (1985) 1291.
19. R.H. Enns, D.E. Edmundson, S.S. Rangnekar, and A.E. Kaplan, *Optical Quantum Electr.* **24** (1992) 1295.
20. R.H. Enns, S.S. Rangnekar, and A.E. Kaplan, *Phys. Rev. A* **36** (1987) 1270.
21. R.L. Burden and J.D. Faires, *Numerical Analysis* 4th ed. (PWS-KENT Publishing Company, Boston, MA, 1989).